Correlations between Dispersion, Acidity, Reducibility, and Propane Aromatization Activity of Gallium Species Supported on HZSM5 Zeolites

ARTICLE *in* THE JOURNAL OF PHYSICAL CHEMISTRY C · FEBRUARY 2010

Impact Factor: 4.77 · DOI: 10.1021/jp910642p

3 AUTHORS, INCLUDING:

Victor De Oliveira Rodrigues
Federal University of Rio de Janeiro
8 PUBLICATIONS **32** CITATIONS
SEE PROFILE

Arnaldo Da Costa Faro Jr.
Federal University of Rio de Janeiro
54 PUBLICATIONS **431** CITATIONS
SEE PROFILE

Correlations between Dispersion, Acidity, Reducibility, and Propane Aromatization Activity of Gallium Species Supported on HZSM5 Zeolites

Victor de O. Rodrigues, Jean-Guillaume Eon, and Arnaldo C. Faro, Jr.*

Instituto de Química—Universidade Federal do Rio de Janeiro, Rio de Janeiro, RJ, Brazil

Received: November 8, 2009; Revised Manuscript Received: January 22, 2010

Gallium-modified ZSM5 zeolites, containing 2, 3, and 4 wt % Ga, were prepared by incipient wetness impregnation with gallium(III) nitrate solutions of HZSM5 samples with SAR values of 24 and 35. The modified zeolites were subjected to two consecutive treatment cycles of reduction in hydrogen and reoxidation in air. The catalysts were characterized by nitrogen physical adsorption, ^{29}Si and ^{27}Al MAS NMR, temperature-programmed reduction, temperature-programmed desorption of ammonia, X-ray absorption spectroscopy, and infrared spectroscopy in the OH stretching region and in the region of skeletal vibrations of adsorbed pyridine. Catalytic activity and selectivity were measured in propane conversion reactions at 703 K. Results were rationalized in terms of correlations among the framework Ga/Al ratio, density, strength and type of acidity, gallium cluster sizes, reducibility of gallium, and propane aromatization activity. It was found that the dispersion of the gallium species was a function only of the framework Ga/Al ratio. Lewis acidity and reducibility of the gallium species were positively correlated with each other and with their degree of dispersion. A correlation was found between propane aromatization activity and the product of the concentrations of strong Lewis and Brønsted acid sites in the oxide form of the catalysts.

Introduction

Aromatization of light alkanes (methane to butane) has been extensively studied because of its economic and strategic importance in terms of the exploitation of natural gas resources and valorization of light hydrocarbons obtained in petroleum refining. Commercially, these reactions using mainly gallium-modified zeolite catalysts of MFI type are named "Cyclar" processes and were developed jointly by UOP and British Petroleum (BP).[1]

Most of these studies date from the 1990s (for a review, see ref 2), but recently, interest in studying these catalysts was renewed[3−13] due to the growing importance of GTL technologies all over the world.

Among the many methods described in the literature for the preparation of Ga/ZSM5 catalysts, surely one of the simplest and most effective from a practical standpoint involves impregnation of the zeolites with aqueous solutions of soluble gallium salts, such as the nitrate, followed by a series of reduction−oxidation cycles, which lead the catalysts to its most active state.[14] It is generally accepted that these cycles are required because (aqua) gallium(III) ions are too large to penetrate the ZSM5 pore network.[14−16] Reduction in hydrogen generates volatile gallium(I) oxide, which then diffuses through the ZSM5 channels to produce dispersed gallium species.[14−16] These dispersed species replace acidic protons of the zeolite framework in an essentially ion-exchange process. It has been stated that these dispersed species are actually gallyl ions adsorbed on exchange positions of the zeolite framework,[6,8,16−18] but experimental evidence for that comes essentially from qualitative interpretation of EXAFS spectra.[6,8,16−18] Furthermore, to our knowledge, there are no systematic studies in the literature about the effects of catalyst composition (silica-to-alumina ratio of the zeolite and gallium content) on the nature of the gallium species obtained in this way and their relation to catalytic activity in alkane aromatization.

Previously,[12] we studied by EXAFS the nature of the gallium species obtained on varying gallium amounts between 2 and 10 wt % in an H-ZSM5 zeolite and its effects on 1-butene aromatization. The catalysts were prepared by impregnation of the zeolite with gallium(III) nitrate solution, followed by successive calcination, reduction in hydrogen, and reoxidation in air. We showed that the increase in gallium content leads to the preferential formation of a segregated β-Ga_2O_3 phase on the external surface of the zeolite and also favors the formation of larger clusters inside its channels, which have low activity in the aromatization reaction. The EXAFS simulations were consistent with an oxidic cluster with four gallium centers. On the other hand, in the case of catalysts with lower gallium amounts, the results were consistent with clusters with a second sphere average coordination number of 1 (Ga−Ga nearest neighbors), which, under reaction conditions, generate the active gallium species in dehydrocycloaromatization reactions. However, the results were based on the characterization of catalysts where gallium was impregnated on a single H-ZSM5 zeolite support.

The main focus of the present work was on the study of the effects of catalyst composition on the nature of the gallium species present in Ga/ZSM5 catalysts prepared by impregnation with gallium nitrate solution and on their catalytic activity in propane aromatization. The rationalization of the results was made in terms of quantitative correlations between the dispersion of the gallium species (estimated from EXAFS measurements), strength and nature of the acid sites (from temperature-programmed desorption of ammonia and infrared spectroscopy of adsorbed pyridine), reducibility of different Ga species (from temperature-programmed reduction), and propane aromatization activity.

* To whom correspondence should be addressed. Phone: +55-21-25627821. Fax: +55-21-25627265. E-mail: farojr@iq.ufrj.br.

10.1021/jp910642p
Published on Web 02/22/2010

Experimental Section

Catalyst Preparation. The HZSM5 type zeolites were supplied by CENPES/PETROBRAS and had two different silica-to-alumina ratios (SAR values): 24 and 35. A sample of silicalite (MFI structured SiO_2) was also used in this study. These zeolites, as received, were subjected to two ion-exchange processes with ammonium chloride solution at 323 K for the minimization of their sodium contents, followed by calcination at 773 K under a 200 mL/min dry air flow for transformation of the ammonium form back into its acidic form.

Gallium was incorporated into these zeolites by incipient wetness impregnation with gallium nitrate solution, in order to obtain three different amounts of this element, ca. 2, 3, and 4 wt % (only the 4 wt % catalyst was prepared in the silicalite series). The impregnated catalysts were calcined at 773 K for 4 h under a 200 mL/min dry air flow.

The gallium-modified zeolites were then subjected to two reduction/oxidation cycles. Reduction was performed under a hydrogen flow of 200 mL/min at 783 K and reoxidation under an air flow of 200 mL/min at the same temperature.

Catalysts used in this work were named using the following scheme: TAGaB, where the letter T refers to the treatments to which the sample was subjected, letter T indicates that it suffered the full treatment described above, letter A refers to the impregnated gallium amount (% wt), and letter B designates the zeolite sample used (Z for ZSM5 and S for silicalite). For ZSM5 catalysts, the letter Z was followed by a number that refers to the SAR of the zeolite. In the case of unmodified zeolite samples, the naming scheme pattern is only TB. For example, the catalyst denoted T3GaZ35 is the catalyst with 3% wt of gallium impregnated in an HZSM5 zeolite with a SAR of 35 and subjected to two reduction/oxidation cycles, and TS is a silicalite sample subjected to the same pretreatments as before.

Textural Characterization. Surface areas and micro-, meso-, and macropore volumes were determined by nitrogen physisorption at 77 K in ASAP 2010 volumetric equipment. Surface areas were calculated by the BET method and micro-, meso-, and macropore volumes by the *t*-plot method.

Prior to nitrogen physisorption analysis, samples were oven-dried at 623 K for approximately 1.5 h and, thereafter, subjected to vacuum pretreatment at 673 K until a degassing rate lower than 2 μm Hg/min was obtained.

Magic-Angle Spinning Nuclear Magnetic Resonance of ^{29}Si and ^{27}Al. Magic-angle spinning nuclear magnetic resonance spectroscopy analyses of ^{29}Si and ^{27}Al were made in a Bruker spectrometer, model DRX-300 (7.05 T). Spectra were obtained with a Bruker CP-MAS multinuclear probe with 4 mm zirconia rotors. Rotation frequencies of 5 and 9 kHz were used for ^{29}Si and ^{27}Al, respectively. The ^{27}Al measurements were made with 6000 scans with pulse intervals of 0.30 s and the ^{29}Si measurements with 1000 scans and pulse intervals of 60s.

Determination of the framework SAR of the catalysts was accomplished by deconvolution of the ^{29}Si NMR $Si(OAl)_n(OSi)_{(4-n)}$ signals using a formula already proposed in the literature[2] and checked against ^{27}Al NMR results.

X-ray Fluorescence. XRF analyses were made in a Rigaku spectrometer, model RIX3100, with a rhodium tube (4 kW). Samples were quantitatively analyzed for SiO_2, Al_2O_3, and Ga_2O_3. Samples were analyzed as self-supported wafers with a catalyst mass of 500 mg.

Temperature-Programmed Desorption of Ammonia (TPD-NH_3). The amount and strength of the acid sites present in the catalysts were determined by temperature-programmed desorption of ammonia (TPD-NH_3) in a dynamic characterization Zeton-Altamira AMI-90 equipment. Initially, the catalysts were dried in situ under He flow at 773 K. Ammonia pulses were then injected at the temperature of 448 K. The temperature-programmed desorption was made under a flow of He between 448 and 773 K, with a heating rate of $\beta = 10$ K·min^{-1} with the ammonia being detected by thermal conductivity (TCD) and quadrupole mass spectrometer (MS) detectors.

Infrared Spectroscopy in the OH Stretching and Adsorbed Pyridine Absorption Regions. These experiments were performed using self-supported wafers of the catalysts, weighing approximately 9 mg, in an infrared cell with CaF_2 windows adapted for in situ treatments. The determination of the infrared spectrum at the OH stretching range was made after sample treatment at 673 K for 4 h under vacuum, and this spectrum was used as background for the adsorbed pyridine experiments. Pyridine was then adsorbed to a 1 Torr equilibrium pressure at 323 K. FTIR spectra were recorded after consecutive evacuation at 323, 373, 423, 473, 573, and 673 K.

X-ray Absorption Spectroscopy. The XAFS spectra (X-ray absorption fine structure) were obtained at the Laboratório Nacional de Luz Síncrotron (Campinas, Brazil), at the gallium K-edge (10367 eV) with transmission detection. The samples were analyzed between 10 300 and 11 300 eV. The standards used as references were gallium nitrate and β-Ga_2O_3, where the latter was used for energy correction of the X-ray beam.

Temperature-Programmed Reduction (TPR). The reducibility of the catalysts was studied by temperature-programmed reduction (TPR) in a dynamic characterization Zeton-Altamira AMI-90 equipment. Initially, the samples were dried in situ under Ar flow at 773 K. Thereafter, the temperature-programmed reduction was performed under a flow of 10% H_2 in Ar between 308 and 973 K, with a heating rate of 10 K·min^{-1}. Finally, the sample was maintained at 973 K for 30 min, enough time for the signal to return to the baseline. Quantification of the H_2 uptake includes this isothermal step.

Catalytic Tests. The catalytic tests for propane conversion were conducted in a batch system with external recirculation of the gas phase at 703 K and atmospheric pressure. The initial partial pressure of propane in the reaction loop was 15 Torr; a known amount of nitrogen was added to the reacting system as an internal standard, and the balance was helium.

The analysis of the reaction mixture was made by periodic sample withdrawal from the gas phase, which was injected in a capillary column of methylsiloxane (100 m × 0.25 mm × 0.5 μm thickness) installed in a Agilent 6890 gas chromatograph equipped with a mass selective detector (quadrupole mass spectrometer), model 5973. Chromatographic area conversion into concentrations was made by means of response factors determined by calibration in our laboratory.

The experiments were performed with approximately 65 mg mass of catalyst, with the exception of the catalytic tests with the pure zeolite samples TZ24 and TZ35, where 200 mg was used due to their low activities.

Results

Catalyst Composition and Textural Properties. The compositions of the synthesized catalysts determined from X-ray fluorescence and MAS ^{29}Si and ^{27}Al NMR are shown in Table 1.

It is first noticed that SAR values measured by XRF were essentially constant within each series of catalysts. The SAR values obtained from ^{29}Si NMR are consistently higher than the ones obtained by XRF, showing that extra-framework aluminum is present in all samples, which is confirmed by the

TABLE 1: Catalyst Composition Determined by X-ray Fluorescence and MAS ^{29}Si and ^{27}Al NMR

catalyst	SAR (XRF)[a]	SAR (NMR)[b]	% O_h Al[c]	% Ga[d]	% Ga (XRF)[e]
TZ35	34.8	38.8	5.6		
T2GaZ35	34.4	40.2	8.2	2	2.0
T3GaZ35	34.6	40.4	10.6	3	3.4
T4GaZ35	35.3	42.4	16.4	4	5.0
TZ24	24.2	32.6	10.3		
T2GaZ24	24.6	35	18.3	2	2.0
T3GaZ24	24.6	34.5	16.1	3	3.7
T4GaZ24	24.2	34.8	16.8	4	4.6
TS	[f]				
T4GaS	[f]			4	4.7

[a] Catalyst SAR determined by X-ray fluorescence. [b] Catalyst framework SAR determined by NMR. [c] Extra-framework aluminum species in octahedral coordination. [d] Impregnated gallium amounts. [e] Catalyst gallium amounts detected by X-ray fluorescence. [f] XRF result: $Al_2O_3 < 0.25$ wt %.

TABLE 2: Textural Characterization Results Determined by Nitrogen Physisorption at 77 K

sample	BET area[a]/m^2 g^{-1}	V_m[b]/cm^3 g^{-1}	V_{MM}[c]/cm^3 g^{-1}
TZ35	391	0.18	0.02
T2GaZ35	356	0.16	0.03
T3GaZ35	331	0.15	0.02
T4GaZ35	335	0.15	0.03
TZ24	388	0.18	0.03
T2GaZ24	324	0.15	0.05
T3GaZ24	329	0.15	0.03
T4GaZ24	324	0.14	0.03
TS	329	0.16	0.23
T4GaS	362	0.15	0.34

[a] Surface area per gram of zeolite. [b] Micropore volume. [c] Meso- and macropore volumes.

^{27}Al NMR results. It should be noticed that the pure zeolites were analyzed after the same reduction−oxidation treatments suffered by the gallium-containing catalysts. The amount of extra-framework aluminum was larger with the gallium-containing catalysts, showing that all catalysts suffered some dealumination due to gallium incorporation. Also in Table 1, it can be observed that impregnated gallium amounts and those determined by XRF are very similar.

Textural characterization results are presented in Table 2. In catalysts series with TZ24 and TZ35, the results show a trend in the reduction of the surface area and micropore volumes with gallium incorporation. This occurs probably due to pore blockage by the deposition of extra-framework gallium and aluminum species within the micropores. No significant modifications were observed in meso- and macropore volumes.

On the other hand, in the case of the materials of the silicalite series, a different picture arises with gallium modification. In these samples, an increase in surface area was observed, which seems to be related mainly with an increase in meso- and macropore volumes because the micropore volume changed very little. A possible explanation is that some debris is removed from the mesopores during impregnation with the gallium nitrate solution.

By and large, textural modifications due to gallium impregnation were modest, showing that the pore structure of the zeolites was largely preserved during catalyst preparation and pretreatment.

Characterization of Acidity. Figures 1−3 show the infrared spectra in the OH stretching region for the catalysts of the TZ35, TZ24, and silicalite series, respectively. In this region, there are three peaks of main interest, which are marked in the figures with vertical lines. The peak at 3611 cm^{-1} is associated with the zeolite Brønsted acid sites, that is, Si(OH)Al bridged sites.

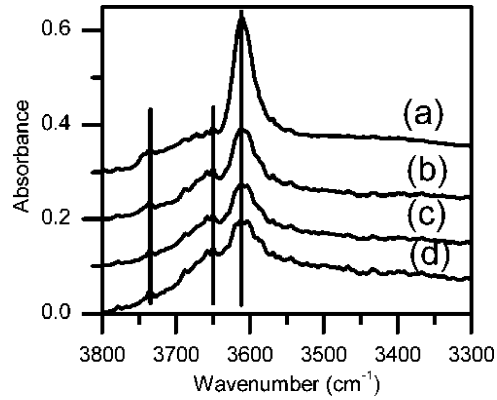

Figure 1. Infrared spectra in the OH stretching region of the TZ35 series: (a) TZ35, (b) T2GaZ35, (c) T3GaZ35, and (d) T4GaZ35. Vertical lines show the position of the peaks with wavenumbers of 3611, 3650, and 3734 cm^{-1}.

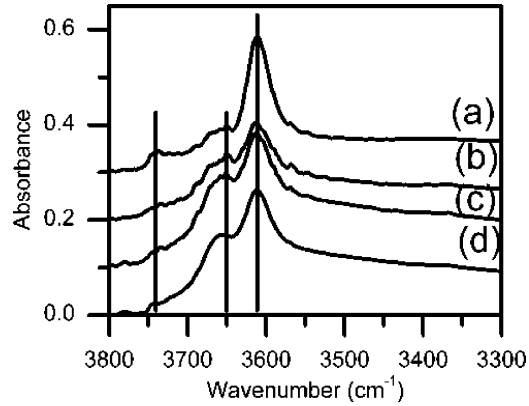

Figure 2. Infrared spectra in the OH stretching region of the TZ24 series: (a) TZ24, (b) T2GaZ24, (c) T3GaZ24, and (d) T4GaZ24. Vertical lines show the position of the peaks with wavenumbers of 3611, 3650, and 3734 cm^{-1}.

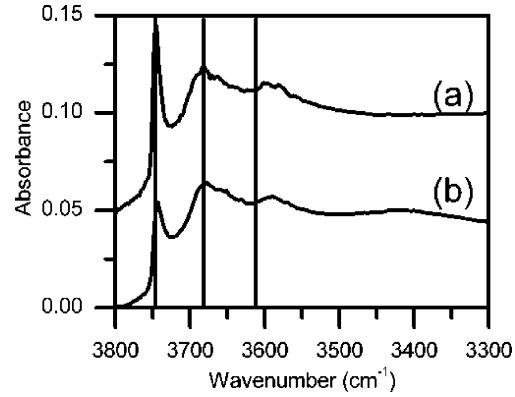

Figure 3. Infrared spectra in the OH stretching region of the silicalite series: (a) TS and (b) T4GaS. Vertical lines show the position of the peaks with wavenumbers of 3611 (peak not present), 3650, and 3734 cm^{-1}.

In Figures 1 and 2, a reduction in intensity of this peak can be observed with increasing gallium content. This has been attributed to the exchange of acidic protons (Brønsted acid sites) with ionic gallium species.[19] In the silicalite series, Figure 3, no peak can be observed at 3611 cm^{-1}, and only a minor feature is observed at 3600 cm^{-1}, which remains undisturbed by gallium impregnation, suggesting that it is not related to Brønsted acidity.

Another important feature is the peak at around 3650 cm^{-1}, usually associated with extra-framework aluminum OH species.[2] In Figures 1 and 2, increase in intensity of this peak is observed

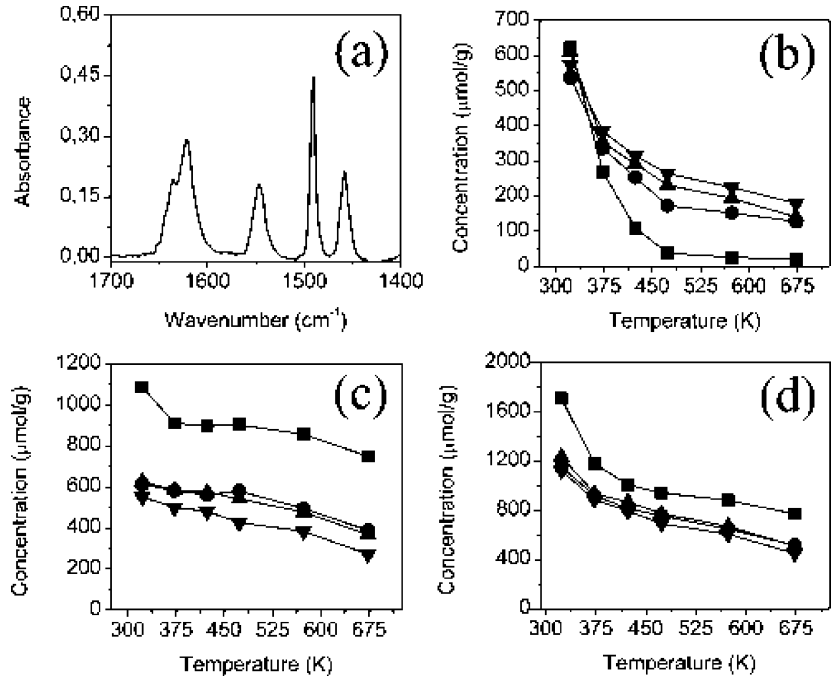

Figure 4. FTIR of adsorbed pyridine for catalysts of the TZ35 series. (a) Spectrum of sample T4GaZ35 after evacuation at 423 K. (b) Lewis acid site concentration. (c) Brønsted acid site concentration. (d) Total acid site concentration. For graphics (b−d): ■, TZ35; ●, T2GaZ35; ▲, T3GaZ35; ▼, T4GaZ35.

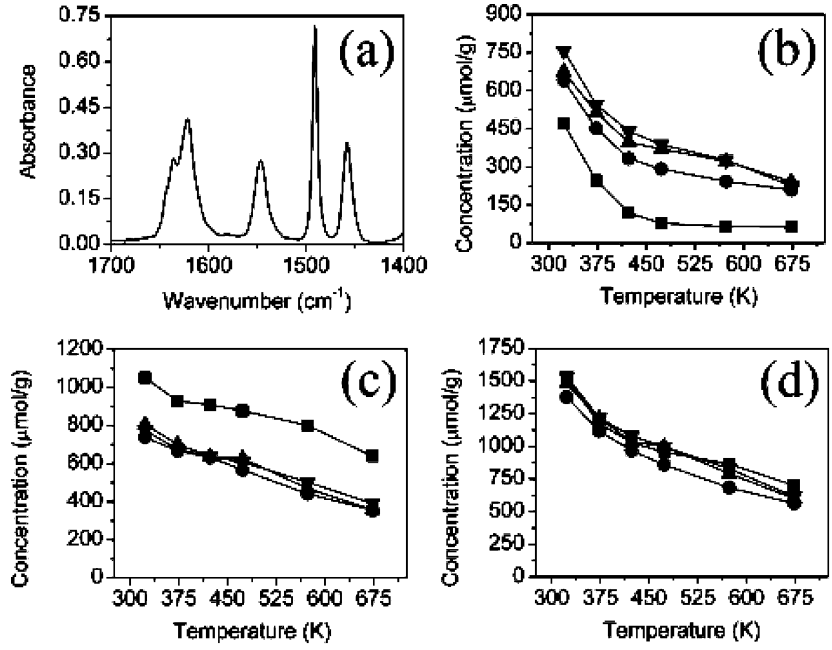

Figure 5. FTIR of adsorbed pyridine for catalysts of the TZ24 series. (a) Spectrum of sample T4GaZ24 after evacuation at 423 K. (b) Lewis acid site concentration. (c) Brønsted acid site concentration. (d) Total acid site concentration. For graphics (b−d): ■, TZ24; ●, T2GaZ24; ▲, T3GaZ24; ▼, T4GaZ24.

with increasing gallium content, which is consistent with the zeolite dealumination observed by solid-state NMR. A peak around 3670 cm^{-1} has been associated with extra-framework gallium OH species.[2] If this band occurs in the spectra of our catalysts at all, it is swamped by the band due to extra-framework alumina. Finally, there is a peak around 3734 cm^{-1} associated with zeolite terminal silanol groups. This peak is much more intense with pure silicalite than it is with the pure HZSM5 materials. This is consistent with the larger meso- and macropore volume observed for silicalite, indicating a more defective crystal structure in this case. It is also interesting to observe that, in the silicalite series, where no Brønsted acid sites exist, gallium appears to interact with silanol terminal groups, as evidenced by the reduction in peak intensity of the silanol band apparent from Figure 3. This cannot be attributed to condensation of silanol groups during thermal treatment because the pure silicalite was subjected to the same treatment as the Ga-modified one.

Figures 4−6 show the results for the pyridine adsorption experiments with the catalysts supported on TZ35, TZ24, and silicalite, respectively, along with a sample spectrum for each catalyst, after evacuation at 423 K. In Figures 4a, 5a, and 6a, the adsorbed pyridine infrared spectra are shown for the 4 wt % samples evacuated at 423 K, in series TZ35, TZ24, and

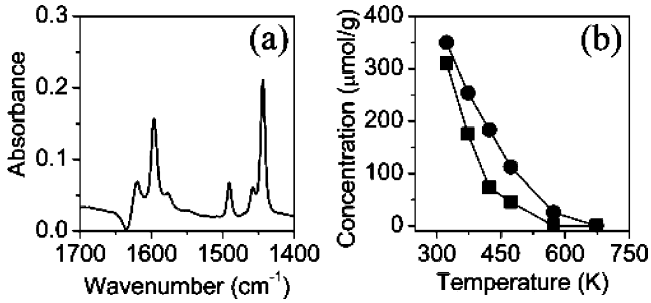

Figure 6. FTIR of adsorbed pyridine for catalysts of the silicalite series. (a) Spectrum of sample T4GaS after evacuation at 423 K. (b) Lewis acid site concentration. For graphic (b): ■, TS; ●, T4GaS.

silicalite, respectively. The bands used in this work to quantify separately the Lewis and Brønsted acid sites were the peaks around 1450 and 1540 cm^{-1}, corresponding to Z-$Ga^{\delta-}Py^{\delta+}$ and Z-O-HPy^+, respectively, the latter being absent in the case of silicalite samples (Figure 6a). In these spectra, peaks at 1490 cm^{-1}, relating to pyridine interacting with Lewis and Brønsted acid sites, and around 1600 cm^{-1} usually associated with pyridine adsorbed on Lewis acid sites, can also be observed.

The Lewis and Brønsted acid site concentration profiles as functions of the evacuation temperature were determined by means of the equations proposed by Emeis.[20] The molar extinction coefficient for pyridine adsorbed as pyridinium ions was determined by considering that, after evacuation between 373 and 473 K, the amount of adsorbed pyridinium ions was essentially constant with the pure zeolites (cf. Figures 4 and 5) and no bridged OH groups could be observed in the appropriate region of the FTIR spectra, indicating complete consumption of acidic protons. The amount of bridged OH groups was considered to equal the amount of framework aluminum in the pure zeolites, as determined by solid-state NMR. An average extinction coefficient was taken from the values obtained with each of the pure zeolites, which differed by ±10% from the average value. The extinction coefficient for pyridine coordinated to Lewis acidic sites was then calculated from the ratio of extinction coefficients for pyridine adsorbed on Brønsted and Lewis sites reported by Emeis.[20]

Figures 4b and 5b show the concentration of pyridine adsorbed on Lewis acid sites as a function of evacuation temperature in the TZ35 and TZ24 catalysts series, respectively. These figures show that, in the parent zeolites, pyridine adsorbed on Lewis acid sites is almost completely removed by evacuation at 473 K. On the other hand, with the gallium-modified materials, pyridine remains adsorbed on the Lewis acid sites at temperatures as high as 673 K in the series with TZ24 and TZ35. This implies that stronger Lewis acid sites than originally present in the zeolite appear as a result of gallium incorporation.

These results are analogous to those of Anunziata et al.[21] on zinc-modified H-ZSM11 zeolite, which indicated the replacement of strong Brønsted acid sites by strong Lewis acid sites. Altwasser et al.[22] and Raischle et al.[23] also studied the acidic properties of gallium-modified HZSM5 catalysts and also found that gallium modification of the zeolite generates high concentrations of Lewis acid sites. The appearance of Lewis acid sites related to extra-framework gallium species was also noticed in the study of gallosilicates by Areán et al.[24] and galloaluminosilicates by Camblor et al.[25] In those cases, extra-framework gallium species were generated by degalliation of the zeolite framework.

In Figure 6b, this same graph is shown for the silicalite series. Although it is observed that Lewis acid site concentration increases more than twice with gallium impregnation (comparison at 423 K), pyridine adsorbed in these sites is almost completely removed by evacuation at 573 K. In other words, no strong Lewis acid sites (defined here as those that retain pyridine at temperatures up to 673 K) are generated upon gallium impregnation on the silicalite sample.

TABLE 3: Acid Site Concentrations Determined by TPD-NH_3 in Samples of the Three Series

catalyst	TZ35	T2GaZ35	T3GaZ35	T4GaZ35
NH_3 desorbed[a]/mmol g^{-1}	0.72	0.68	0.69	0.69
catalyst	TZ24	T2GaZ24	T3GaZ24	T4GaZ24
NH_3 desorbed[a]/mmol g^{-1}	0.94	0.87	0.87	0.91
catalyst	TS	T4GaS		
NH_3 desorbed[a]/mmol g^{-1}	0.12	0.10		

[a] Ammonia desorbed in the TPD experiment up to 773 K.

Figures 4c and 5c show that gallium incorporation decreases Brønsted acid site concentration in both TZ35 and TZ24 series of catalysts, agreeing with the previously shown infrared results in the OH stretching region. It is observed that, in both cases, the fraction of the pyridine adsorbed at 473 K remaining adsorbed on Brønsted sites after evacuation at 673 K is smaller with the gallium-containing samples than with the pure zeolite; that is, the Brønsted sites remaining in the gallium-modified material are weaker than the ones originally present in the zeolite. This is in agreement with earlier reports in the literature by Raischle et al.,[23] Altwasser et al.,[22] Mériaudeau et al.,[26] and Kanazirev et al.[27] in gallium-modified ZSM5 and by Anunziata et al.[21] in zinc-modified ZSM11 catalysts.

Finally, Figures 4d and 5d show the total acid site concentration as function of the treatment temperature, where it can be seen that, for the SAR 35 series, there is a small decrease in the total acid site concentration with gallium impregnation, whereas for the SAR 24 series, total acid site concentration remains almost the same. This means that gallium incorporation largely results in converting Brønsted acid sites associated with the zeolite framework into Lewis acid sites, associated with the incorporated gallium species.

Table 3 shows the acid site concentrations in all catalysts determined by TPD-NH_3, and Figure 7 shows the profiles obtained for samples of the TZ24 and TZ35 series.

The acid site concentrations in H-ZSM5 zeolites can be used to estimate their SAR, if it is assumed that each molecule of desorbed ammonia corresponds to an aluminum atom in the zeolite framework, that is, that there is no ammonia adsorbed on Lewis acid sites. For the zeolites with framework SARs of 32.6 and 38.8, the values obtained were, respectively, 30 and 40, indicating that, indeed, in the original zeolites, acid sites are largely of the Brønsted type. This is corroborated by FTIR of adsorbed pyridine because, at 448 K, the temperature at which the ammonia pulses were injected in the TPD experiments, essentially all of the pyridine has desorbed from Lewis acid sites; cf. Figures 4−6.

The results in Table 3 indicate that the concentrations of acid sites determined by ammonia desorption are almost constant along each series, showing only a small decrease with gallium incorporation. On the other hand, Figure 7 shows that gallium incorporation decreases strong acid site concentration with an increase in the weak acid site concentration.

A parallel may be drawn between the adsorbed pyridine and ammonia TPD results for series with TZ24 and TZ35. From

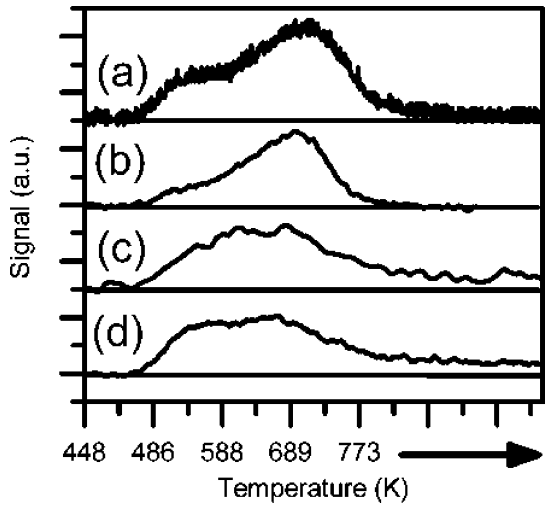

Figure 7. TPD-NH_3 graphical results of the TZ24 and TZ35 series with $\beta = 10$ K/min: (a) TZ24, (b) TZ35, (c) T3GaZ24, and (d) T3GaZ35.

Figures 4c and 5c, it is clear that most of the pyridine remaining on the parent ZSM5 materials after evacuation at 473 K is not removed even after evacuation at 673 K. On the other hand, the Ga-containing materials have a smaller total amount of pyridine adsorbed on Brønsted acid sites and a large proportion of it is removed after evacuation at 673 K. The increase in the proportion of the weaker acid sites observed in the NH_3 TPD can thus be correlated with the increase in the weaker Brønsted acid sites proportion observed in the infrared spectra of adsorbed pyridine. The peaks around 3650 cm^{-1} observed in the hydroxyl stretching region of the FTIR spectra (Figures 1 and 2), assigned to extra-framework aluminum and/or extra-framework gallium hydroxyls,[2] could be associated with these weaker Brønsted acid sites. It is also possible that gallium incorporation perturbs the acidic strength of neighboring Brønsted sites. The fact that the total concentration of acid sites measured by ammonia desorption is nearly constant with respect to gallium incorporation, while the amount of pyridine adsorbed on Brønsted sites decreases, may be explained by the difference in basicity between the two probe molecules: possibly some ammonia desorption in the Ga-containing catalysts occurs at 473 K from Brønsted acid sites that cannot adsorb pyridine at this temperature.

In the case of the silicalite series, the TPD results confirm the FTIR ones in that both show the presence of only weak acid sites.

Probably the most interesting result of the TPD experiments is the fact that, as opposed to what happens with the parent zeolites, the signal does not return to baseline at the end of temperature program, this effect being observed in all gallium-modified catalysts in series with TZ24 and TZ35. Coupling of the TPD equipment to a mass spectrometer showed that it was indeed ammonia desorbing from the samples at the end of the temperature programming. This indicates that gallium incorporation causes the appearance of some stronger acid sites than those present in the parent zeolites. This can be correlated to the appearance of strong Lewis acid sites with gallium incorporation in the zeolite observed in the pyridine adsorbed infrared experiments. These strong Lewis acid sites are not observed in the gallium-modified silicalite sample, and consequently, their appearance depends on the existence of Brønsted acid sites in the parent zeolite samples.

EXAFS Characterization. As discussed above, infrared spectroscopy in the OH stretching region and in the region of adsorbed pyridine supports the idea that gallium species replace zeolite Brønsted acid sites and shows that strong Lewis acid sites are generated by gallium incorporation; however, they do not provide any information about the nature of the gallium species present in the catalysts. With this objective in mind, extended X-ray absorption fine structure (EXAFS) was used.

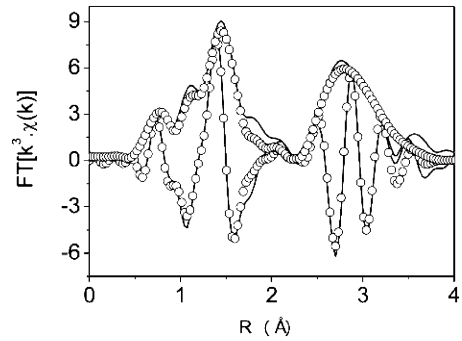

Figure 8. Fourier transform magnitude and imaginary part of the β-Ga_2O_3 EXAFS spectrum: experimental, line; simulation, ○.

The EXAFS spectra were analyzed using the IFEFFIT software.[28] Structural parameters were obtained by simulation with a Levenberg−Marquadt algorithm in *R*-space using theoretical phase and amplitude functions generated by the FEFF 8.20 software.[29,30] The optimized parameters were defined as usual.[31]

Some important structural parameters could be obtained by the simulation of the EXAFS spectrum of β-Ga_2O_3. Figure 8 shows the experimental spectrum along with the simulated one, whereas Table 4 shows the fitting results.

The simulation was accomplished in *R*-space with a *k* range between 2−15 $Å^{-1}$, an *R* range between 1−3.4 Å, and was based on the crystallographic data available for the β-Ga_2O_3 phase.[32] This phase contains two different gallium sites in an asymmetric unit cell, one with tetrahedral and the other with octahedral coordination geometry. The Ga−O bond lengths are in the range of 1.83−1.86 Å within the tetrahedral sites and are longer in the octahedral sites, 1.93−2.07 Å. The O atoms have a distorted cubic close-packed structure, and the crystallographic point group is *C*2/*m* with unit cell parameters $a = 12.214$ Å, $b = 3.0371$ Å, $c = 5.7981$ Å, and $\beta = 103.83°$.[32] Also, gallium is evenly distributed between the two nonequivalent sites of tetrahedral and octahedral coordination. In our model, for the β phase, both sites were used, and the *x* factor in Table 4 refers to the fraction of gallium sites in tetrahedral coordination (ideally $x = 0.5$ in the β phase).

It is important to notice that the corrections to the scattering path length parameters, ΔR_Γ, were calculated from equations deduced for each scattering path from the crystal structure, as functions of the unit cell parameters (*a*, *b*, and *c*) and corrections applied (δa, δb, and δc). Debye−Waller factors σ^2_Γ were calculated using the equation of movement algorithm implemented in the FEFF 8.20 software[29,30] and force constants obtained from the literature.[33]

From Table 4, the good quality of the simulation can be assessed, bearing in mind that the deviations of the unit cell parameters (δa, δb, and δc) are all small compared with the values reported in the literature and that the proportion between tetrahedral and octahedral sites is very close to the theoretical value of 50%. It is worth emphasizing that the value obtained experimentally for the parameter S_0^2 is equal to the value obtained theoretically by the FEFF 8.20 software[29,30] using an ab initio method.

TABLE 4: β-Ga_2O_3 EXAFS Spectra Simulation Results

S_0^{2a}	E_0^a	a^b (δa^c)	b^b (δb^c)	c^b (δc^c)	$x^{a,d}$ (%)	R_{Factor} (%)
0.95 (0.03)	−2.1 (1.5)	12.21 (0.01)	3.04 (−0.04)	5.80 (0.22)	51 (3)	3.4

[a] Associated errors are between parentheses. [b] Unit cell parameters for β-Ga_2O_3 (Å). [c] Absolute experimental deviations of the unit cell parameters (Å). [d] Proportion of tetrahedral gallium sites.

TABLE 5: EXAFS Spectra Analysis Results: Interatomic Distances, Coordination Numbers, and Debye−Waller Factors

sample	$N_O^{a,c}$	σ^2_{Ga-O} (Å^{-2})^{a,d}	R_{Ga-O} (Å)^{a,b}	$N_{Ga}^{a,c}$	R_{Ga-Ga} (Å)^{a,b}	σ^2_{Ga-Ga} (Å^{-2})^{a,d}	R_{Factor} (%)
T2GaZ24	4.0 (0.3)	0.0066 (0.0007)	1.83 (0.02)	0.65 (0.07)	3.00 (0.01)	0.010 (0.005)	3.3
T2GaZ35	4.1 (0.3)	0.0068 (0.0007)	1.84 (0.02)	0.96 (0.10)	3.00 (0.01)	0.013 (0.003)	3.1
T3GaZ24	4.1 (0.3)	0.0070 (0.0009)	1.84 (0.01)	1.22 (0.10)	3.00 (0.01)	0.013 (0.003)	3.9
T3GaZ35	4.0 (0.2)	0.0069 (0.0007)	1.84 (0.03)	1.55 (0.15)	3.00 (0.01)	0.013 (0.003)	3.8
T4GaZ24	4.0 (0.2)	0.0067 (0.0008)	1.83 (0.02)	1.74 (0.20)	3.01 (0.01)	0.013 (0.003)	2.9
T4GaZ35	4.0 (0.3)	0.007 (0.001)	1.83 (0.02)	1.73 (0.20)	3.00 (0.01)	0.013 (0.003)	4.0
T4GaS	3.9 (0.2)	0.0036 (0.0004)	1.814 (0.004)	2.00 (0.20)	2.90 (0.08)	0.021 (0.011)	2.2
$Ga(NO_3)_3$	6.2 (0.4)	0.005 (0.002)	1.96 (0.05)				0.2

[a] Associated errors can be found between parentheses. [b] Ga−O and Ga−Ga atomic distances in Å. [c] Mean coordination number for single scattering path. [d] Debye−Waller factor for single scattering path.

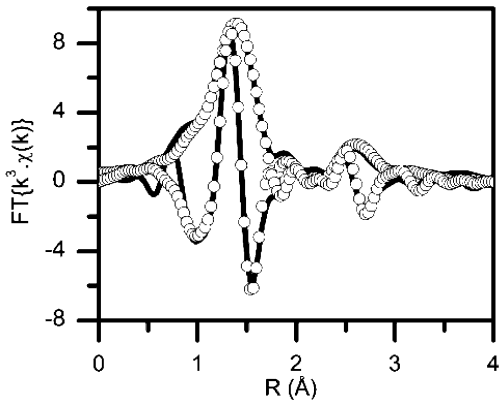

Figure 9. Fourier transform magnitude and imaginary part of the T4GaZ24 EXAFS spectrum: experimental, line; simulation, ○.

The EXAFS spectral simulations of the samples were based on a model where gallium is found under the form of oxidic clusters inside the zeolite channels. Table 5 shows the simulation results in *R*-space using *k* between 2 and 12 Å^{-1}, dk = 2, k_{weight} = 3, and *R* between 1 and 3.1 Å. Fitting results for the gallium nitrate standard first coordination shell are also shown in Table 5, as an assessment on the simulation method used. Values for the R_{Factor} obtained were all in the range between 2 and 4%, indicating the good quality of the simulations. Figure 9 shows the results of the simulation compared to the experimental spectrum in the case of sample T4GaZ24, which is representative of the results obtained.

The results shown in Table 5 clearly indicate the growth of the gallium oxide clusters, evidenced by the increase in the second sphere coordination numbers (Ga neighbors) with increasing gallium content and also a trend to the formation of larger clusters with increasing SAR.

No evidence was found for the presence of bulk gallium(III) oxide in any of the catalysts. In β-Ga_2O_3, there is a 1:1 ratio of octahedrally to tetrahedrally coordinated Ga^{3+} species, which gives an average first sphere coordination number of 5 (oxygen atoms), whereas a value close to 4 (tetrahedral coordination) was found for samples in all catalysts. Furthermore, the second sphere average coordination number in β-Ga_2O_3 is 5, whereas the largest second coordination number found here was 2. This shows that the gallium species in our catalysts are highly dispersed. In fact, in at least one case, an average coordination number significantly smaller than 1 was obtained, indicating that atomically dispersed oxidic gallium species are present in the catalysts. Finally, as stated earlier, average bond lengths for tetrahedral gallium species are in the range between 1.83 and 1.86 Å and for octahedral species are in the range between 1.93 and 2.07 Å, whereas those obtained for all catalysts synthesized in this work were 1.83 ± 0.02 Å, which can be clearly associated with tetrahedral gallium species. Moreover, in the case of the gallium nitrate standard, the Ga−O bond length of 1.96 ± 0.05 Å can be correctly associated with octahedral gallium species, as expected.

Thus, the picture that emerges from the EXAFS data for the HZSM5-supported catalysts is that of small oxidic gallium clusters and atomically dispersed oxidic gallium species, where the gallium is tetrahedrally coordinated by oxygen atoms. It should be emphasized here that the EXAFS spectra were obtained with catalyst samples exposed to air, so hydration or hydrolysis of the supported gallium species is to be expected.

It should also be noticed that the EXAFS observation of aluminum ligands at the gallium second coordination sphere is very difficult because of the poor scattering power of aluminum as compared with gallium, the relatively large Ga−Al distances, bearing in mind this low scattering probability, and the high structural disorder associated with Ga−Al distances.

TPR Experiments. TPR measurements were made to investigate the reducibility of gallium species in the catalysts, since it is generally assumed that the active species is under reduced form.[5−8,10,11,13,25−27] In Figure 10, the reduction profiles for samples in the series with TZ35 are shown. In this figure, a shift of the reduction maxima toward higher temperatures can be seen with increasing gallium content (maxima at 861, 896, and 938 K, for catalysts T2GaZ35, T3GaZ35, and T4GaZ35, respectively). The catalysts in the TZ24 series showed analogous results, which were omitted here for reasons of space.

Table 6 shows the numerical results related to the TPR analysis regarding the catalysts of both series. An increase in hydrogen uptake with decreasing zeolite SAR and increasing gallium content in the catalysts is clearly apparent. Furthermore, an increase in the reducibility of gallium is observed (represented by the number of moles of hydrogen consumed per mole of impregnated gallium) with decreasing amount of impregnated gallium and decreasing SAR.

A small peak may be noticed in the TPR profiles for all catalysts, with a maximum at ca. 340 K. The origin of this peak is uncertain at the moment, but it could be due to activated hydrogen chemisorption.

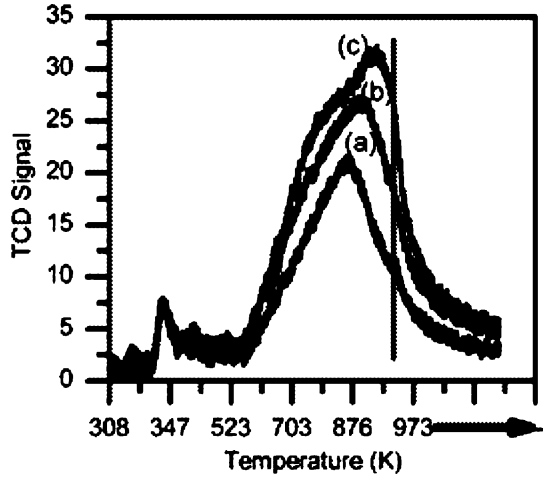

Figure 10. TZ35 series catalyst reduction profiles: (a) T2GaZ35, (b) T3GaZ35, and (c) T4GaZ35. The vertical line delimits the beginning of the isothermal step at 973 K.

TABLE 6: Number of Moles of Hydrogen Consumed Per Sample Mass and Impregnated Gallium Number of Moles

catalyst	μmol H_2/g sample[a]	nH_2/Ga[b]
T2GaZ35	237	0.83
T3GaZ35	305	0.62
T4GaZ35	384	0.54
T2GaZ24	305	1.06
T3GaZ24	328	0.62
T4GaZ24	393	0.60

[a] Micromoles of hydrogen consumed per gram of sample during reduction up to 973 K. [b] Moles of hydrogen consumed per mole of gallium (XRF) during sample reduction up to 973 K.

TABLE 7: Catalytic Activity: Initial Reaction Rates of Propane Conversion and Transformation to Alkanes, Olefins, and Aromatic Hydrocarbons

catalyst	$-r_0$ (C_3H_8)[a,b]	r_0 (alkane)[a,c]	r_0 (olefin)[a,c]	r_0 (aromatics)[a,c]
TZ35	23.9	6.5	14.8	1.7
T2GaZ35	525	42	160	370
T3GaZ35	430	31	37	357
T4GaZ35	479	48	132	311
TZ24	24.3	12.8	11.6	0.0
T2GaZ24	671	47.6	173	475
T3GaZ24	592	73.6	54.0	484
T4GaZ24	700	70.2	64.6	575

[a] Initial activities expressed in 10^{-7}mol·(g·min)$^{-1}$. [b] Initial reaction rate of propane conversion. [c] Initial reaction rates of propane conversion to alkanes, olefins. and aromatic hydrocarbons.

No reduction was observed in the gallium-modified silicalite sample in TPR experiments up to 973 K, although significant reduction was observed at higher temperatures.

Catalytic Activity and Selectivity. In propane aromatization reactions over our catalysts, the products obtained are saturated and olefinic hydrocarbons in the range between C_1 to C_4 and aromatic hydrocarbons in the range between C_6 and C_8. Table 7 shows the results of initial activity for propane total conversion and for conversion to alkanes, olefins, and aromatics, whereas Figure 11 shows the moles of propane converted to each of the three classes of compounds as a function of contact time for the catalysts TZ35 and T3GaZ35.

There was considerable scatter in the results for the pure zeolites due to the small conversions attained. Results for other catalysts were omitted for simplicity, as they are analogous to these. The initial rates of conversion of propane to olefinic, saturated, and aromatic hydrocarbons were obtained from the slope of the curves analogous to those of Figure 11 at zero reaction time. Initial rates of propane conversion were obtained in a similar way, from curves of moles of propane versus time.

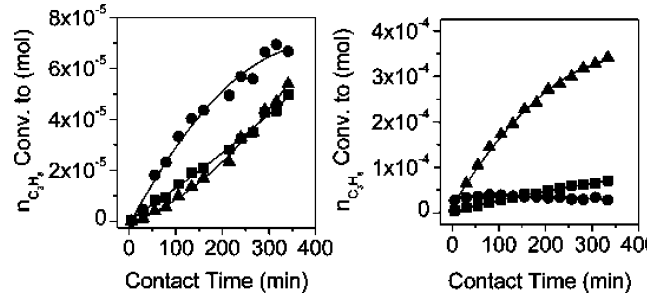

Figure 11. Number of moles of propane converted to alkanes, olefins, and aromatics: A, TZ35; B, T3GaZ35; ■, alkanes; ●, olefins; ▲, aromatics.

From the data reported in Table 7, it can be observed that initial rates of propane conversion are at least 20 times higher for gallium-containing catalysts than for the respective zeolite but are almost independent of gallium content. Considering only the aromatization activities, gallium impregnation leads to catalysts approximately 200 times more active in the case of the TZ35 series (in the case of the TZ24 series, initial aromatization activity was essentially zero with the parent zeolite). The main primary products of the reaction with the zeolite TZ35 are olefins (initial rates of formation of saturated and aromatic hydrocarbons are very small).

This is consistent with the generally accepted view that, in the pure zeolite, the main route for aromatic hydrocarbon production is intermolecular hydride transfer after the initial dehydrogenation of an alkane, while gallium modification of the zeolite introduces an additional dehydrogenation route to alkane aromatization.

It is beyond the scope of the present paper to discuss the detailed product distributions obtained, which have been discussed many times before. Here, the main focus is on structure−activity correlations for propane aromatization on gallium-modified ZSM5 catalysts.

Discussion

As mentioned in the Introduction, it is generally accepted[14−16] that incorporation of gallium into H-ZSM5 by impregnation with gallium nitrate solutions requires successive reduction−oxidation cycles because (aqua) gallium(III) ions are too large to penetrate the ZSM5 pore network. Reduction in hydrogen generates volatile gallium(I) oxide, which then diffuses through the ZSM5 channels to produce dispersed gallium species. Repetition of the reduction−oxidation cycles then improves the gallium distribution and dispersion.[14−16]

Second sphere coordination numbers (nearest-neighbor gallium atoms) obtained here from EXAFS measurements show that isolated oxidic gallium species are, by no means, the only species present, although an average coordination number considerably smaller than one in at least one case shows that these isolated species do indeed occur. One question is how does the composition of the gallium-modified catalyst influence the dispersion of the oxidic gallium species?

Figure 12 shows that a single curve is able to correlate the second sphere coordination number (N_{Ga}), measured by EXAFS, with the gallium-to-framework aluminum ratio (Ga/Al_{FW}) ratio in the zeolites, as measured by X-ray fluorescence (Ga) and NMR spectroscopy (Al_{FW}) for all catalysts.

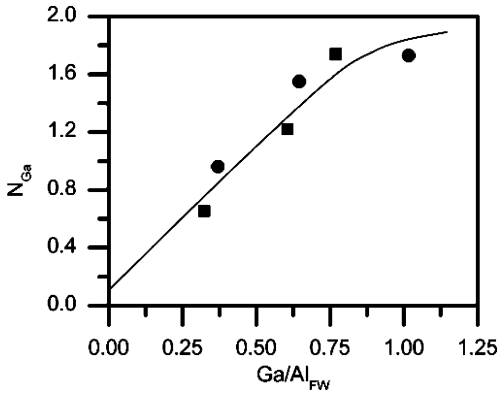

Figure 12. Correlation between the second sphere coordination number (N_{Ga}) with the Ga/Al$_{FW}$ ratio in the zeolites: ■, TZ24 series; ●, TZ35 series.

The initial portion of this curve seems to be fairly linear and to extrapolate to close to the origin of the graph, implying that, in the limit of 0 Ga/Al$_{FW}$ ratio, only isolated oxidic gallium species exist in the catalysts ($N_{Ga} = 0$). However, for any finite gallium content, oxidic gallium clusters are formed. In the opposite direction, the curve seems to level off to a limiting value, which must be related to the largest possible oxidic gallium cluster inside the zeolite channels. From the results in Figure 12, the limiting value for N_{Ga} is around 2, but this does not necessarily represent the maximum second sphere coordination number for the gallium atoms, as more dispersed species, such as dimeric[12] ($N_{Ga} = 1$) and isolated oxidic gallium species ($N_{Ga} = 0$), must contribute to the average value.

Because of the formation of oxidic gallium clusters, Brønsted acid sites remain in the catalysts even for Ga/Al$_{FW}$ ratios equal to 1. Figure 13a shows the number of Brønsted acid sites (defined as the amount of pyridinium ions retained on each catalyst after evacuation at 473 K) per aluminum atom in the catalysts versus the Ga/Al$_{FW}$ atomic ratio.

It is seen that, after an initial decrease as compared to the parent zeolites, this number remains nearly constant with increasing Ga content. Because the second sphere coordination number of the gallium atoms increases with increasing Ga/Al$_{FW}$ ratio, this indicates that oxidic gallium clusters do not replace acidic protons in the zeolite framework.

For comparison, the number of Brønsted acid sites per framework aluminum obtained by integration of the bridged-hydroxyl band in the FTIR spectra of the materials is shown in Figure 13b. Again, an average molar extinction coefficient for this band was estimated from the spectra of the parent zeolites, assuming a 1:1 ratio of $OH_{Bridged}$/Al$_{FW}$. It is clearly apparent that the same behavior is deduced from both panel a and panel b in Figure 13.

Figure 14 shows the number of strong Lewis acidic sites, that is, those retaining pyridine after evacuation at 673 K, per gallium atom in the catalysts, as a function of the second sphere coordination number, N_{Ga}. It is clear that this number decreases with increasing N_{Ga} and a single line appears to correlate the data for both series of catalysts. Therefore, strong Lewis acidity is related to the presence of highly dispersed gallium species, very likely, the same gallium species that are capable of exchanging with the acidic protons of the zeolite framework.

The first sphere coordination number of gallium (nearest-neighbor oxygen atoms) was close to 4 with all ZSM5-supported catalysts (cf. Table 5). However, it should be remembered that coordination numbers were obtained by EXAFS with the catalysts as received, whereas the acidity measurements were made after evacuation at high temperature. Therefore, the 4-fold coordinated isolated gallium species may be converted to strong Lewis acid sites, probably coordinatively unsaturated gallyl species, during high-temperature treatment, for example, as follows:

$$\cdots Ga(OH)_2^+ \rightarrow \cdots Ga{=}O^+ + H_2O$$

The results shown in Table 4 for the silicalite-supported catalyst, together with the ones in Figure 6, show that this catalyst does not fit the correlation shown in Figure 14, as the second sphere coordination number is nearly the same as that found with the GaZSM5 catalysts, yet it presents neither Brønsted nor Lewis acid sites capable of retaining pyridine up to 673 K. This is certainly because, in this catalyst, there are no isolated oxidic gallium species, as there are essentially no aluminum sites in the parent support to allow their formation.

Another property that was dependent on the composition of the catalysts (zeolite SAR and Ga loading) is the reducibility of gallium, as shown in Table 6 in terms of hydrogen uptake per gallium atom. It should be stressed that no reduction of the silicalite-supported material was observed up to the final temperature used with the other materials (973 K), although reduction did occur at higher temperatures. Because the second sphere coordination number, N_{Ga}, was a function only of the Ga/Al$_{FW}$ ratio in the catalysts, we attempted to see whether there would be some unifying correlation between reducibility and N_{Ga}. Figure 15 shows that, indeed, such a correlation exists, with increasing reducibility for decreasing N_{Ga}, showing that highly dispersed oxidic gallium species are more reducible than oxidic gallium clusters.

Because the same trend is observed with respect to the Lewis acidity of the gallium species, a correlation is then also to be expected between the reducibility of gallium and the number of strong Lewis acid sites per gallium atom. Figure 16 shows that, as expected from the other correlations, this does, in fact, exist, except in this case, it is linear, within the range of the parameters explored, and extrapolates to very close to the origin. It is, furthermore, noticed that the slope of this line is very close to 2.

It should be remembered that the silicalite-supported material is not reduced up to the temperatures used with the ZSM5-supported catalyst and does not display any strong Lewis acidity, so it actually corresponds to the origin in Figure 16.

The correlation between reducibility and strong Lewis acidity most likely arises from the fact that this type of acidity promotes the dissociation of hydrogen on a strong Lewis acid−base pair for the reduction of gallium. Furthermore, strong Lewis acidity is inversely correlated with the dispersion of the oxidic gallium species. This, taken together with the slope close to 2 obtained for the line in Figure 16, is consistent with the following reduction process:

$$\cdots Ga{=}O^+ + 2H_2 \rightarrow \cdots GaH_2^+ + H_2O$$

Formation of a gallium hydride species by hydrogen reduction of zeolite-supported gallium has been reported before in the literature.[34,35]

There is not a general agreement on the species responsible for the activation of alkanes in Ga-modified ZSM-5 catalysts. Proposals found in the literature include gallyl ions,[6,8,16−18,36] isolated Ga^+ ions,[6,7,11,16,37] isolated gallium hydride species,[5,17,38]

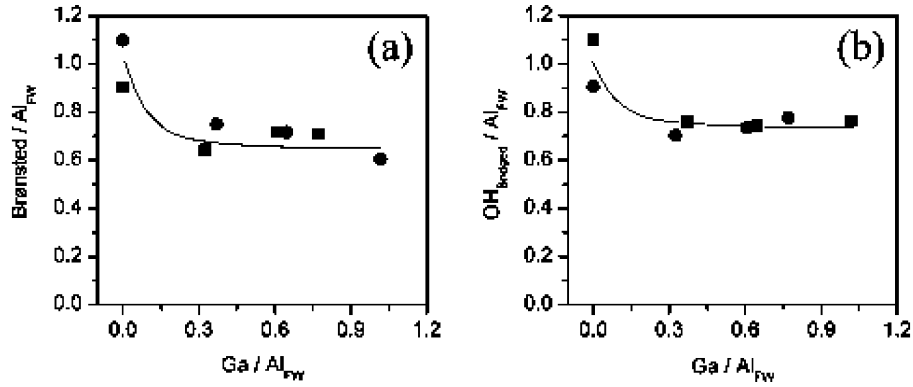

Figure 13. (a) Strong Brønsted acid site concentration per aluminum atom and (b) bridged hydroxyl groups per aluminum atom vs the Ga/Al$_{FW}$ atomic ratio: ■, TZ24 series; ●, TZ35 series.

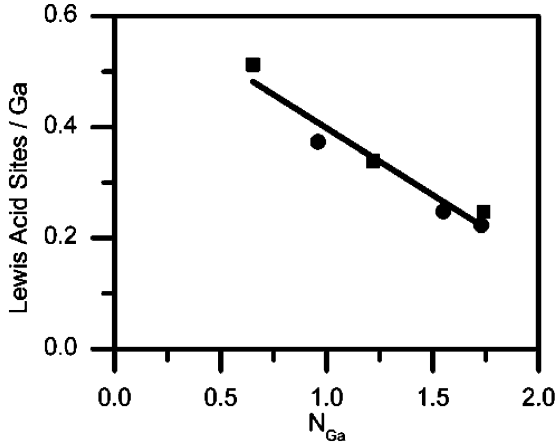

Figure 14. Correlation between strong Lewis acid site concentration per gallium atom in the catalysts and gallium second sphere coordination number: ■, TZ24 series; ●, TZ35 series.

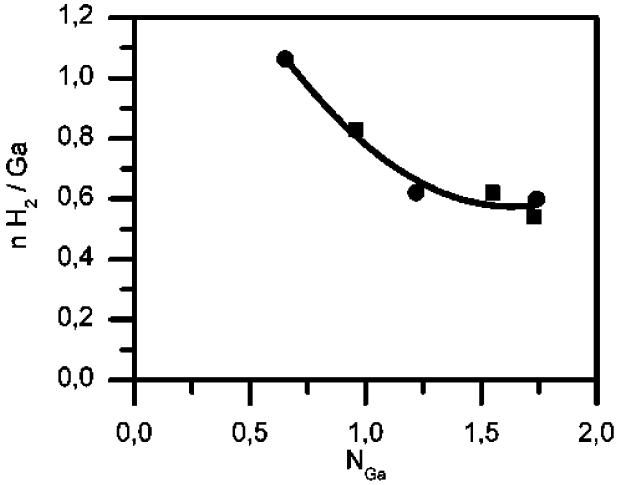

Figure 15. Gallium phase reducibility (nH$_2$/Ga) vs the gallium species per gram of sample: ■, TZ24 series; ●, TZ35 series.

and gallium hydride oligomers.[39−41] Our own results,[13] using a pulse method, showed that, although the oxidized form of the catalyst has the capability of converting propane, the propane conversion per pulse increases with increasing number of pulses. At the same time, the amount of hydrogen eluted from the catalyst rises from a small value in the first pulse to a limiting value of one hydrogen molecule per molecule of propane converted. This strongly suggests that a reduced gallium species is mainly responsible for the catalytic activity and is formed upon exposure of the oxidized catalyst to propane. As our results

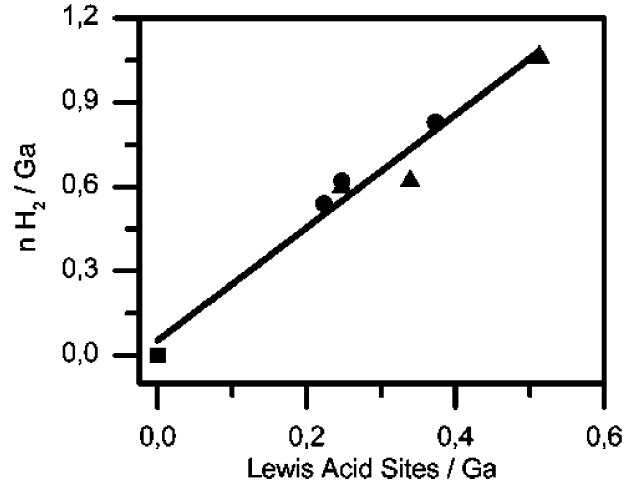

Figure 16. Correlation between reducibility of gallium phase (nH$_2$/Ga) and the number of strong Lewis acid sites per gallium atom: ▲, TZ24 series; ●, TZ35 series; ■, silicalite series.

presented here showed that the reducibility of gallium increases with increasing Lewis acidity, some correlation is expected between alkane activation activity and Lewis acidity of the catalysts. Even if gallyl species are responsible for alkane activation, this would be most likely related to their Lewis acidity, so the correlation between activity and Lewis acidity would be expected to hold also in this case.

At the same time, Brønsted acid sites, even if not necessarily directly involved in alkane activation, are required at least for the oligomerization and cyclization reactions that eventually lead from dehydrogenated hydrocarbon species initially produced from the alkane to aromatic hydrocarbons. Therefore, the simultaneous presence of Lewis and Brønsted activity is required for alkane aromatization reactions.

If this is so, some correlation should be expected between aromatization activity and the product of strong Lewis by strong Brønsted acidity, estimated here from the amount of pyridine retained in the catalysts on each type of site after evacuation at 673 K. Figure 17 shows that a fairly linear correlation indeed seems to exist that extrapolates very close to the origin, which includes the experimentally measured pure zeolites and the Ga-modified silicalite. It should be stressed that the line shown in the graph is the best line obtained by least-squares fitting.

Conclusion

Our results shed light on the nature of the gallium species produced in Ga-modified ZSM-5 catalysts prepared by impreg-

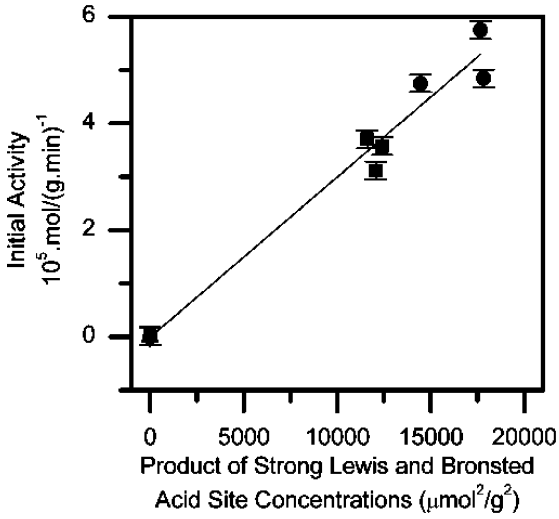

Figure 17. Correlation between aromatization activity and the product of the Lewis and Brønsted strong acidity: ■, TZ35 series; ●, TZ24 series; ▲, silicalite series.

nation with gallium(III) nitrate solution, followed by several reduction−oxidation cycles, and on the effect of the zeolite silica-to-alumina ratio (SAR) and gallium loading on the dispersion of these species. It was found that isolated oxidic gallium species exist in the catalysts, along with condensed species, but their concentration increases with decreasing Ga/Al_{FW} ratio. A single function seems to correlate the degree of aggregation of the oxidic gallium species and the Ga/Al_{FW} ratio, irrespective of the zeolite SAR.

Gallium incorporation, besides decreasing the density of Brønsted acid sites as compared with the pure zeolites, caused the appearance of strong Lewis acid sites, capable of retaining adsorbed pyridine up to 673 K. This strong Lewis acidity is related to the presence of highly dispersed oxidic gallium species, probably gallyl ions bound to ion-exchange sites of the zeolite framework. These species, perhaps on account of their strong Lewis acidity, are more easily reduced than the condensed gallium species present in the zeolite channels.

A fairly linear correlation was found between the initial rate of propane aromatization at 703 K and the product of strong Lewis and Brønsted acid site concentrations. This points toward the need of the simultaneous existence of Lewis and Brønsted acid sites in the oxidized form of the catalysts for alkane aromatization activity. Rather than attributing that exclusively to the cooperative action of Lewis and Brønsted acid sites in the reaction mechanism, we believe that the reducibility of the strong Lewis acid species facilitates the formation of the reduced gallium species that is the actual active site in alkane activation. Brønsted acid sites are required for the oligomerization reactions involved in aromatization, although our results do not exclude the possibility that they participate in the initial alkane activation step as well.

Acknowledgment. The authors would like to thank the PRONEX "Funcionalização de Hidrocarbonetos" for financial support, Dr. Yiu Lau Lam of CENPES/PETROBRÁS for ZSM5 zeolite samples, the "Laboratório Nacional de Luz Síncrotron" (Campinas, Brazil) for project D04B-XAFS1 7653 approval and for financial support during X-ray absorption measurements, NUCAT/COPPE/UFRJ for XRF analysis, and LABRMN/IQ/UFRJ for MAS ^{29}Si and ^{27}Al NMR analysis. V.d.O.R. would like to thank CAPES for a doctorate scholarship. J.-G.E. thanks CNPq for financial support during this work.

References and Notes

(1) Mowry, J. R.; Anderson, R. F.; Johnson, J. A. *Oil Gas J.* **1985**, *83*, 128.
(2) Fricke, R.; Kosslick, H.; Lischke, G.; Richter, M. *Chem. Rev.* **2000**, *100*, 2303.
(3) Pereira, M. S.; Nascimento, M. A. C. *Chem. Phys. Lett.* **2005**, *406*, 446.
(4) Choudhary, T. V.; Kinage, A.; Banerjee, S.; Choudhary, V. R. *Catal. Commun.* **2006**, *7*, 166.
(5) Pereira, M. S.; Nascimento, M. A. C. *J. Phys. Chem. B* **2006**, *110*, 3231.
(6) Rane, N.; Overweg, A. R.; Kazansky, V. B.; Van Santen, R. A.; Hensen, E. J. M. *J. Catal.* **2006**, *239*, 478.
(7) Lukyanov, D. B.; Vazhnova, T. *Appl. Catal., A* **2007**, *316*, 61.
(8) Pidko, E. A.; Hensen, E. J. M.; Van Santen, R. A. *J. Phys. Chem. C* **2007**, *111*, 13068.
(9) Zhidomirov, G. M.; Shubin, A. A.; Milov, M. A.; Kazansky, V. B.; Van Santen, R. A.; Hensen, E. J. M. *J. Phys. Chem. C* **2008**, *112*, 3321.
(10) Pidko, E. A.; Hensen, E. J. M.; Zhidomirov, G. M.; Van Santen, R. A. *J. Catal.* **2008**, *255*, 139.
(11) Rane, N.; Kersbulck, M.; Van Santen, R. A.; Hensen, E. J. M. *Microporous Mesoporous Mater.* **2008**, *110*, 279.
(12) Faro, A. C., Jr.; Eon, J.-G.; Nogueira, L.; Rodrigues, V. O.; Silva, R. F. *Catal. Today* **2008**, *133−135*, 913.
(13) Faro, A. C., Jr.; Rodrigues, V. O. In *Studies in Surface Science and Catalysis*; Gedeon, A., Massiani, P., Babboneau, F., Eds.; Elsevier: Amsterdam, The Netherlands, 2008; Vol. 174B, p 1155.
(14) Mériaudeau, P.; Abdul-Hamid, S. B.; Naccache, C. *J. Catal.* **1993**, *139*, 679.
(15) Biscardi, J. A.; Iglesia, E. *Catal. Today* **1996**, *31*, 207.
(16) Nowak, I.; Quartararo, J.; Derouane, E. G.; Védrine, J. C. *Appl. Catal., A* **2003**, *251*, 107.
(17) Frash, M. V.; Van Santen, R. A. *J. Phys. Chem. A* **2000**, *104*, 2468.
(18) Himei, H.; Yamadaya, M.; Kubo, M.; Vetrive1, R.; Broclawik, E.; Miyamoto, A. *J. Phys. Chem.* **1995**, *99*, 12461.
(19) García-Sanchez, M.; Magusin, P. C. M. M.; Hensen, E. J. M.; Thiine, P. C.; Rozanska, X.; Van Santen, R. A. *J. Catal.* **2003**, *219*, 352.
(20) Emeis, C. A. *J. Catal.* **1993**, *141*, 347.
(21) Anunziata, O. A.; Pierella, L. B. *Catal. Lett.* **1993**, *19*, 143.
(22) Altwasser, S.; Raischle, A.; Traa, Y.; Weitkamp, J. *Chem. Eng. Technol.* **2004**, *27*, 1262.
(23) Raischle, A.; Moser, S.; Traa, Y.; Hunger, M.; Weitkamp, J. *Catal. Commun.* **2001**, *2*, 23.
(24) Areán, C. O.; Bonelli, B.; Palomino, G. T.; Safont, A. M. C.; Garrone, E. *Phys. Chem. Chem. Phys.* **2001**, *3*, 1223.
(25) Camblor, M. A.; Perez-Pariente, J.; Fornes, V. *Zeolites* **1992**, *12*, 280.
(26) Mériaudeau, P.; Naccache, C. *Appl. Catal.* **1991**, *73*, L13.
(27) Kanazirev, V.; Price, G. L.; Dooley, K. M. In *Studies in Surface Science and Catalysis*; Jacobs, P. A., Jaeger, N. I., Kubelková, L., Wichterlová, B., Eds.; Elsevier: Amsterdam, The Netherlands, 1991; Vol. 69, p 277.
(28) Newville, M. *J. Synchrotron. Radiat.* **2001**, *8*, 322.
(29) Rehr, J. J. *Rev. Mod. Phys.* **2000**, *72*, 3.
(30) Ankudinov, A. L.; Ravel, B.; Rehr, J. J.; Conradson, S. D. *Phys. Rev. B: Condens. Matter Mater. Phys.* **1998**, *58*, 7565.
(31) Faro, A. C., Jr.; Souza, K. R.; Eon, J.-G.; Rocha, A. B.; Leitão, A. A.; Capaz, R. *Phys. Chem. Chem. Phys.* **2003**, *5*, 3811.
(32) Ahman, J.; Svensson, G.; Albertsson, J. *Acta Crystallogr., Sect. C: Cryst. Struct. Commun.* **1996**, *52*, 1336.
(33) Lucazeau, G.; Dohy, D.; Revcolevschi, A. *J. Solid State Chem.* **1982**, *45*, 180.
(34) Kazansky, V. B.; Subbotina, I. R.; Rane, N.; van Santen, R. A.; Hensen, E. J. M. *Phys. Chem. Chem. Phys.* **2005**, *7*, 3088.
(35) Kazansky, V. B.; Subbotina, I. R.; van Santen, R. A.; Hensen, E. J. M. *J. Catal.* **2005**, *233*, 351.
(36) Hensen, E. J. M.; García-Sánchez, M.; Rane, N.; Magusin, P. C. M. M.; Liu, P.-H.; Chao, K.-J.; van Santen, R. A. *Catal. Lett.* **2005**, *101*, 79.
(37) Price, G. L.; Kanazirev, V.; Dooley, K. M.; Hart, V. I. *J. Catal.* **1998**, *173*, 17.
(38) Iglesia, E.; Meitzner, G. D. *J. Catal.* **1993**, *140*, 209.
(39) Chao, K. J.; Wei, A. C.; Wu, H. C.; Lee, J. F. *Microporous Mesoporous Mater.* **2000**, *35−36*, 413.
(40) Rozanska, X.; Sánchez, M. G.; Hensen, E. J. M.; Van Santen, R. A. *C. R. Chim.* **2005**, *8*, 509.
(41) Chao, K. J.; Liu, P.-H. *Catal. Surv. Asia* **2005**, *9*, 11.

JP910642P